AVCO EVERETT RESEARCH LABORATORY

a division of
AVCO CORPORATION

EXPERIMENTAL INVESTIGATION OF COLLISION-FREE SHOCKS AND PLASMAS

R. M. Patrick and M. Camac

RESEARCH REPORT 122
Contract No. AF 49(638) 61
September 1961

prepared for

AIR FORCE OFFICE OF SCIENTIFIC RESEARCH
OFFICE OF AEROSPACE RESEARCH
UNITED STATES AIR FORCE

EXPERIMENTAL INVESTIGATION OF COLLISION-FREE SHOCKS AND PLASMAS

by

R. M. Patrick and M. Camac

AVCO-EVERETT RESEARCH LABORATORY
a division of
AVCO CORPORATION
Everett, Massachusetts

Contract No. AF 49(638)-61

September 1961

prepared for

AIR FORCE OFFICE OF SCIENTIFIC RESEARCH
OFFICE OF AEROSPACE RESEARCH
UNITED STATES AIR FORCE
Washington, D.C.

Project No. 9751
Task No. 37510

ABSTRACT

Investigation of the structure of a shock wave provides an excellent opportunity for studying the dissipation processes in collision-free plasmas. The thickness of collision-free shock waves was previously obtained from measurements of the light emitted by the plasma in a magnetic annular shock tube. The magnitude of the shock thickness, and its Mach number and density dependence were in agreement with a theoretical estimate based on the concept that the required dissipation in the shock is produced by nonlinear interactions between magnetohydrodynamic waves.

Further confirmation of these results has been obtained. A. Measurements of the magnetic field have shown that the magnitude of the field change across the shock agrees with that expected from the conservation equations. Also the distance over which the field changes agrees with the previous shock thickness measurements. B. The electron temperature was estimated to be above 10 electron volts based on the ultraviolet radiation intensity and the ratio of bound-bound and free-free radiation. C. Measurements of the heat transfer from the plasma to the shock tube wall indicates that less than 1/10 of the gas energy is dissipated to the walls; thus, there is good containment of the shock heated plasma for a time large (50 times) compared to the shock rise transit time.

The results of these experiments show that the collision-free thickness is inversely proportional to the Alfven Mach number of the shock. The radiation emitted by the shock heated plasma has been measured over a large range in plasma density; these results, together with those for the magnetic field jump across the shock, show that the performance of the MAST can be predicted by a theory which assumes infinite plasma conductivity.

INTRODUCTION

The objective of the experiments described in this paper is to create a magnetohydrodynamic[1, 2, 3] shock wave which produces a plasma in which 1) the collision mean free path is longer than any length in the apparatus, 2) the ion cyclotron radius is small compared to the size of the container, 3) the plasma behind the shock is completely ionized, and 4) the plasma energy density is of the order of the magnetic energy density. A laboratory experiment which produces this plasma requires a magnetic field strength of the order of 10 to 20 kilogauss, a particle density of the order of 10^{15} particles per cm^3, and a temperature of the order of $10^{6}{}^{o}K$. A completely ionized gas is required with high kinetic temperatures; thus, hydrogen was chosen as the working fluid, because the simple structure of this atom permits complete ionization at relatively low energies per particle. A temperature of $10^{6}{}^{o}K$ generated by a shock wave requires a very high shock speed. Therefore, magnetic fields were used to furnish the driving force and containment of the shock heated plasma.

The requirements of magnetic containment and a constant driving force through a uniform channel led to the development of a magnetic annular shock tube, MAST (see Fig. 1). Details of its operation are presented.[4, 5] The container for the working gas is formed by the annular space between two concentric cylinders.[6, 7, 8] The driving force which produces the shock wave is furnished by the azimuthal magnetic field due to radial currents in the annulus. These radial currents are created by discharging a capacitor bank connected to the electrodes. When the gas between the electrodes breaks down, the capacitors are discharged through the gas and this provides the radial drive current. The space between the two cylinders was evacuated, and during the experiments hydrogen was allowed to pass through an annular passage around an insulating spacer between the electrodes and through the annulus to a pumping system. This flow system provided a means of obtaining a low impurity level (500 parts per million).

For all the experiments described in this paper, there was an initial

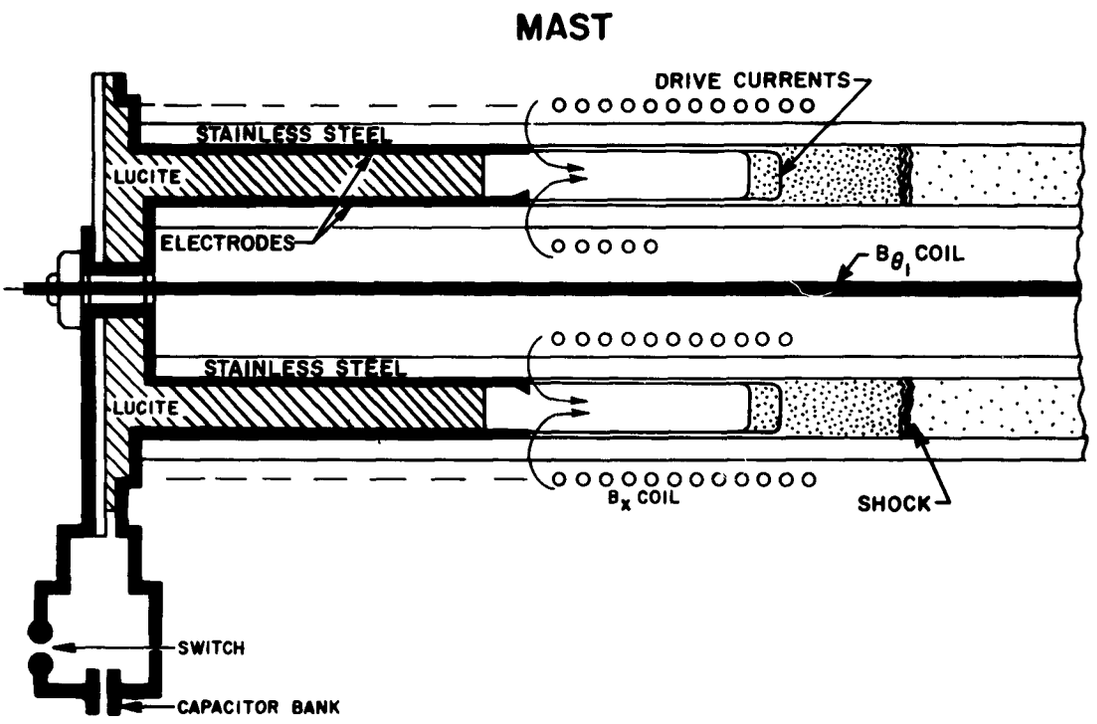

Fig. 1 This is a cross sectional view of the MAST. The drawing is not to scale. The B_x coils consist of two concentric solenoids denoted by the small circles. The B_θ bias field is produced by a current in the conductor along the axis.

magnetic bias field ahead of the shock composed of both an azimuthal component, B_{θ_1}, and a small axial component, B_x. The bias fields were furnished by two coil configurations shown in Fig. 1. The magnitude of B_{θ_1} was sufficient to cause a hydrogen ion moving with the same velocity as the shock to have a gyro-radius that is smaller than the channel width (i.e., annulus spacing). This is an experimentally determined criterion[4] for obtaining high speed shocks in excess of 2.5×10^7 cm/sec.

In order to experimentally establish the existence of high speed shocks, measurements were made of the shock velocity, the plasma density and magnetic field jumps across the shock, and heat transfer[3] to the side walls behind the shock. The measurements of the shock velocity and plasma densities have been reported previously[4] and these results agree with the theoretical values[5] based on the measured drive magnetic field intensity and conditions ahead of the shock. Recently, the change in the magnetic field has been measured with a new type of flux coil.[9] These measurements verify that there is a compression of the magnetic field across the shock which checks the calculated value[5] and also gives shock thickness in agreement with the radiation results reported previously. Furthermore, a new type of heat transfer gauge has been developed[3] which has a sufficiently fast response time to measure the wall heat transfer due to the shock heated plasma during the experimental test time ($\frac{1}{2}$ to 2μ sec). The heat transfer measurements show that about 90% of the plasma energy is contained which verifies the use of the energy conservation across the shock.

The shock waves described in this paper are propagating into room temperature hydrogen. The energy invested in dissociation and ionization to completely dissociate and ionize hydrogen is 7.5 electron volts per particle. This is to be compared to an enthalpy of over 500 electron volts per particle behind the shock. The ionization process can play a role only in the front portion of such high speed shock waves, since the dissipation energy necessary to cause the jump conditions is much larger than the ionization energy. The major portion of the shock structure must involve a mechanism which is much more energetic than an ionization process.

Experimental Results

MAST Development: Recently, some modifications have been made to the MAST which have improved its performance. A larger MAST with a mean diameter of 30 cm has been constructed with a channel spacing equal to 2.1 cm and a 1.5 meter useful length. The ratio of the channel width to the mean radius is equal to 0.14 for the 30 cm MAST compared to a ratio of 0.30 for the 15 cm MAST.[4] The two concentric cylinders which form the annulus have been constructed of stainless (non-magnetic) steel, instead of glass with mylar and brass liners.[4] The stainless steel wall is in contact with the plasma. Higher energy densities in the shock heated plasma can be attained. The two concentric electrodes (Fig. 2) are insulated from the stainless steel channel walls by thin layers of mylar. The mylar sleeves extend about 3 mm beyond the electrodes. The gas in the vicinity of the electrodes is preionized before the main drive field switch is closed. This preionization is accomplished in two steps; the first is due to a relatively low current radial discharge between the electrodes due to a radial electric field, E_r. The second stage is an induced azimuthal discharge due to a large oscillating azimuthal electric field, E_θ.

The first stage of the preionization is accomplished by discharging a small capacitor across the annulus between the electrodes. The current from this discharge is critically damped and has the same sign as the current from the main discharge, that is, the cathode is the center electrode; the anode is the outside electrode. The total maximum current from this radial discharge is of the order of 100 amps; and the time required to reach current maximum is about 0.3μsec. This current is sufficiently low to prevent large body forces acting on the ionized hydrogen plasma which would propel the ionized plasma away from the electrodes before the main discharge can take place.

Within 0.4μsec after the E_r breakdown, a 500 $\mu\mu$f capacitor is discharged through a three turn E_θ coil which is embedded in the lucite separator between the electrodes. The frequency of this discharge is of the order of 10^7 cycles per second and the oscillating voltage on the coil during the discharge is approximately 10^5 volts. This oscillating current in the

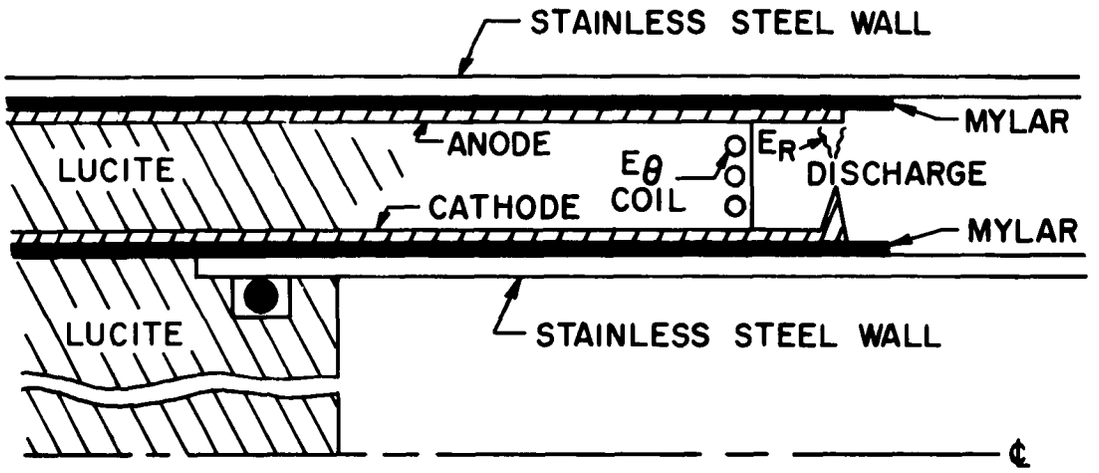

Fig. 2 This is a cross sectional view of the electrode configuration in the MAST. The drawing is not to scale. The electrodes are insulated from the two stainless steel cylinders which make up the MAST walls by thin sheets of mylar. The E_θ coil is connected to a small (500 $\mu\mu$f), high voltage (100 kv) capacitor through leads which pass through the lucite separator between the electrodes.

coil induces an azimuthal electric field, E_θ, between the electrodes which is sufficiently strong to break down the hydrogen gas in the vicinity of the coil around the annulus. Within 1 μsec after the initiation of the E_r discharge, the main bank switch is closed.

This empirically determined procedure produces a uniform discharge from the main bank around the annulus at the electrodes. This is the best technique we have developed to date, to produce a uniform shock which propagates at the velocity predicted[5] from the conservation equations and the initial conditions in the shock tube. It must be pointed out, however, that this procedure does not produce a shock with the theoretical[5] velocity every time the tube is discharged. It is felt, at the present time, that our inconsistent results are due to the lack of control of the breakdown processes across the annulus downstream from the electrodes.

Shock Velocity: The shock velocities have been determined by measuring the time interval between the arrival of the shock at several axial stations. The shock was identified by the onset of plasma radiation, and more recently, by the magnetic field change across the shock and the onset of plasma heat transfer to the side walls. These new results give shock velocities in agreement with the radiation results and further verify the use of the momentum equation to predict the shock velocities.

Density Ratio Across Shock: The plasma density behind the shock waves has been obtained by measuring the intensity of the radiation emitted by the shock heated plasma, Fig. 3. Plasma radiation emitted in the direction normal to the shock tube axis was observed. Quartz windows (1.27 cm diameter) were aligned flush with the inside wall of the outer tube. Radiation with wave lengths between 3750A and 6600A was measured with a photomultiplier interference filter system having a bandwidth of about 80A. In addition, a spectrograph consisting of two quartz lenses and a water prism was used, for measurements from 3400A to 4400A. Ultraviolet radiation from about 300A to 1200A was also measured with a tungsten photoelectric detector.[10]

It has been shown[4] that the visible radiation emitted by the shock heated plasma is proportional to N_e^2, where N_e is the electron density.

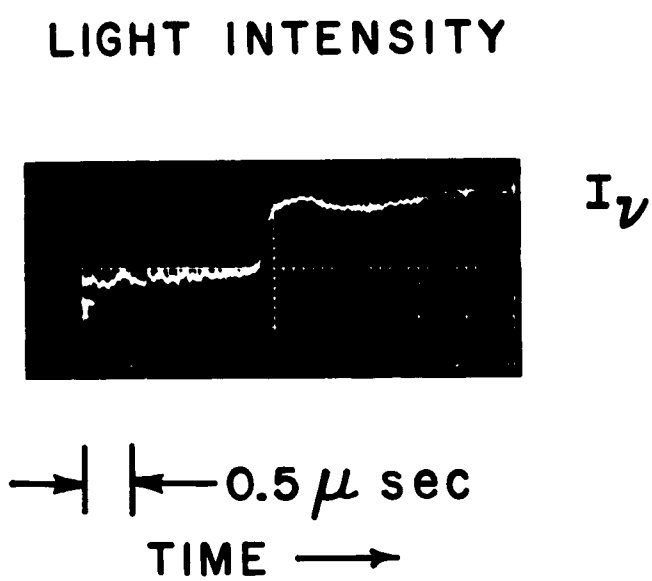

Fig. 3 This oscillogram was obtained by monitoring the plasma radiation at 4400A; the vertical deflection of the trace is proportional to light intensity. The sudden onset of radiation marks the arrival of the shock at the viewing station.

This intensity is due predominantly to free-free radiation for electron temperatures above 10 ev. The experiments reported previously were carried out for low initial pressures in a MAST, where the final equilibrium energy per particle behind the shock is large compared to the energy necessary to ionize and dissociate the hydrogen. Recently, the range of initial gas pressure has been extended to include conditions behind the shock where the energy per particle is not large compared to the ionization energy. A summary of these results showing the measured radiation at 4400A is given in Fig. 4. These experiments were carried out with a value of the ratio B_1/B_0 equal to 0.4 (where B_1 and B_0 are the magnitudes of the magnetic fields ahead of the shock and behind the drive currents, respectively), so that the Alfven Mach number, M_A, (shock velocity divided by the Alfven velocity ahead of the shock) was 2 and the density ratio across the shock was 2.2.

For these conditions the radiation for p_1 below 200μ is due predominantly to free-free transitions.[11] For higher initial pressures, free-bound radiation[12] makes a significant contribution and must be taken into account. The calculated curve for the intensity was based on equilibrium conditions behind the shock. The drop in the calculated curve for p_1 greater than 400μ is due to incomplete ionization behind the shock.

These results show that within the scatter of the data the measured radiation agrees with the expected value up to 800μ. For p_1 greater than 800μ the calculated plasma conductivity is low enough to allow the magnetic field to diffuse from the interface to the shock during the test time. This indicates that the assumption of infinite conductivity in the shock for p_1 greater than 800μ is no longer valid.

It should be noted that for low initial pressures the experiments agree with the theoretical prediction and that for these conditions the radiation measurements furnish a good determination of the electron density behind the shock.

Δ B Measurements: The change in the magnetic field across the shock was measured with small single turn coils[9,13], see Fig. 5, that were inserted through the outer wall and centered in the annulus. The diameter of the coils ranged from 0.4 mm to 7 mm; the wire size from 0.085 mm to 0.25 mm. Both insulated and bare coils were used. The output of the

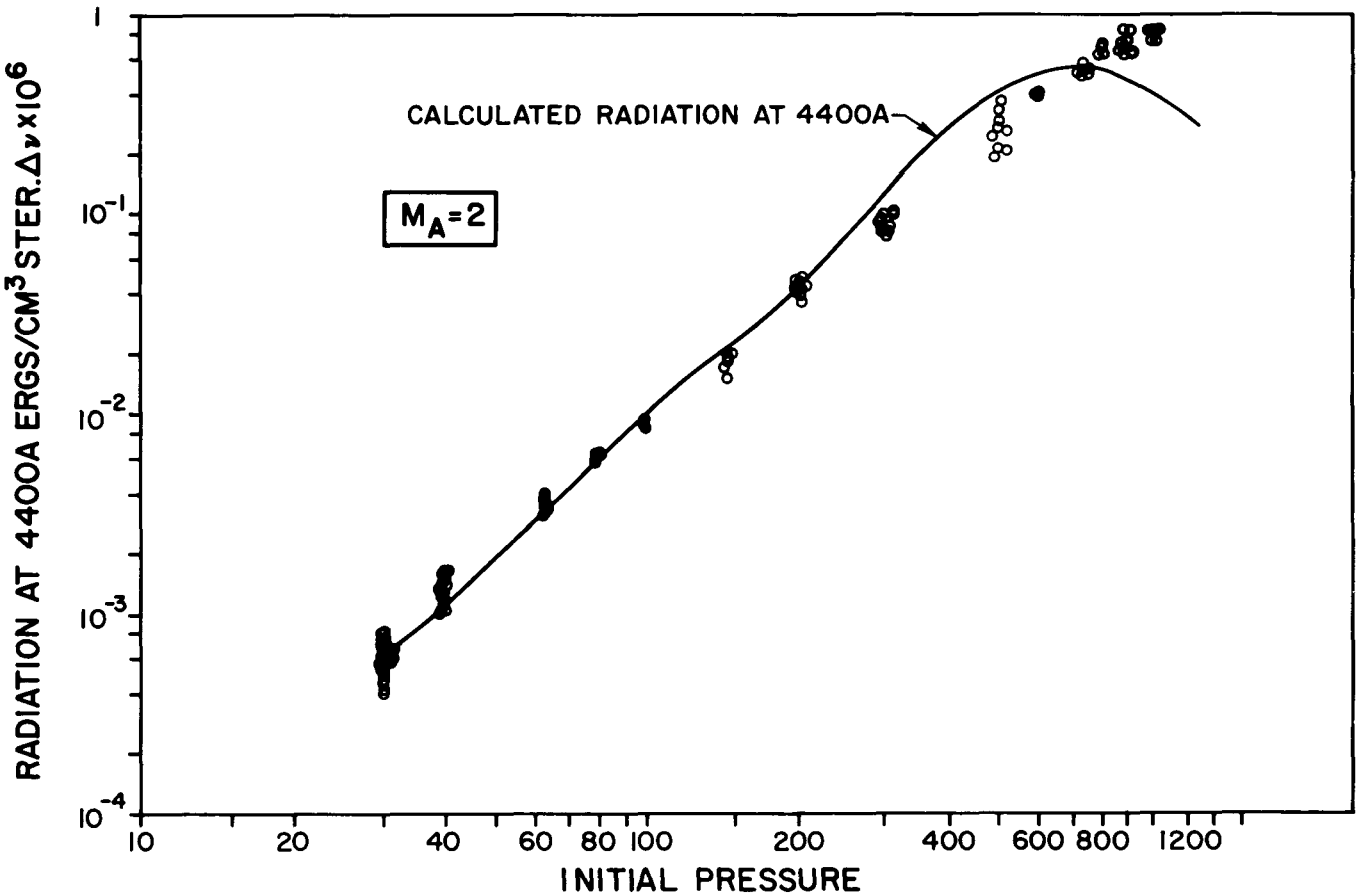

Fig. 4 This is a plot of the measured plasma radiation intensity per cm^3 ster. $\Delta\nu$ at 4400A versus the initial pressure in microns. An interference filter was used with a bandwidth of approximately 70A. The Alfven Mach number was held constant ($M_A = 2$). These results were obtained using the interference-filter and photomultiplier system.

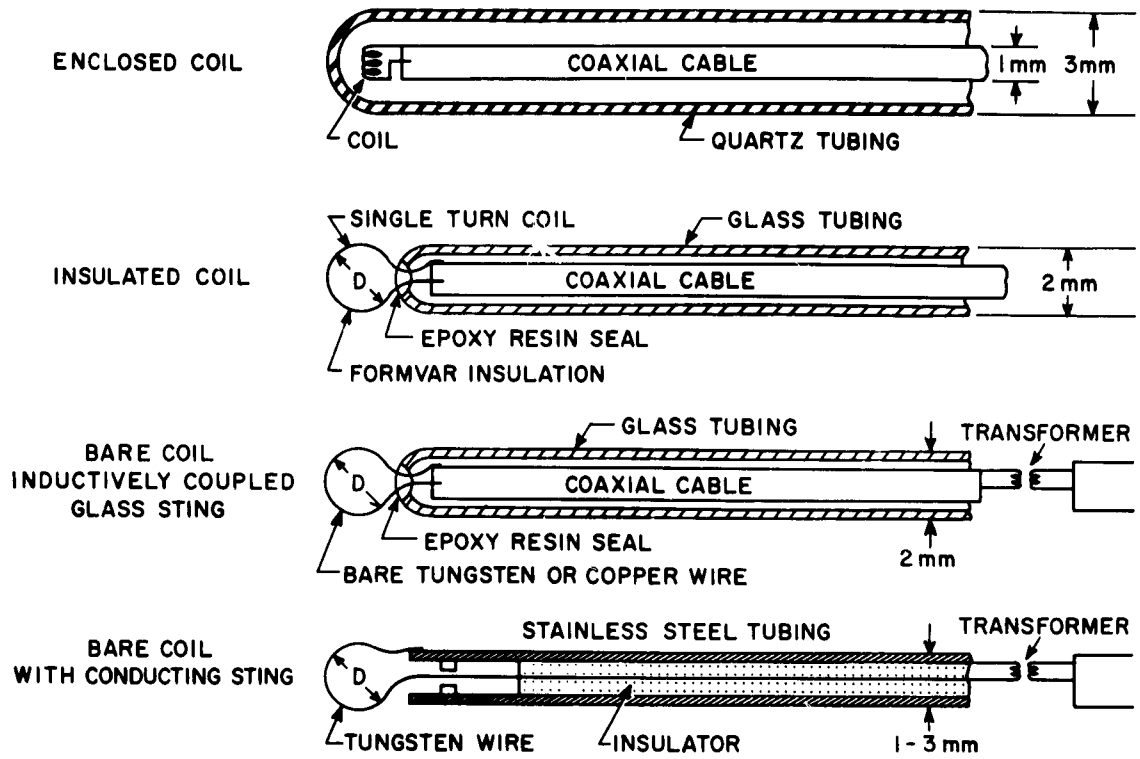

Fig. 5 These coil configurations were used to measure the changes in the magnetic field across the shock. The quartz enclosed coils (top design) were unsuccessful in measuring this change, because the plasma which flowed outside the quartz, was shielded from the coil. The other three diagrams show exposed coils; all of these correctly measured the magnetic field jumps across the shock. The insulated single turn coil was covered with (three coats of) formvar enamel. The bare coils were in electrical contact with the plasma. The results obtained with both the glass and steel mounting stings were essentially the same. The diameter, D, of these coils ranged from .4 mm to 7 mm; the diameter of the steel tubing for the bottom configurations ranged from 1 to 3 mm.

insulated coil went directly to an oscilloscope, while the bare coils were inductively coupled to isolate the large plasma potential from the oscilloscope. An oscillogram obtained by using the directly-coupled insulated coil is shown in Fig. 6. The oscillogram shows both the signal due to the time derivative of the B_θ field in the coil (bottom trace) and the integrated signal showing the compression of the B_θ field across the shock (top trace). The coil frequency response was determined from 5×10^6 to 4×10^8 cycles per second by using a calibrated sinusoidal magnetic field. The uniform field region of a Helmholtz coil geometry was used and a known sinusoidal current was passed through the Helmholtz coils. This calibration showed that the coil response in free space was linear for frequencies up to 1.2×10^8 cycles per second.

The bare coils were used in order to decrease the ablation from the coil surface arising from the intense plasma heat transfer. A series of experiments have been performed which show that the ablation products become ionized presumably in the boundary layer about the coil and electrically shield the coil. In the extreme case where a 1 mm coil was enclosed in a small glass tubing, Fig. 5, top drawing, there was no reproducible magnetic flux signal at the time of shock passage. The tubing was larger than the size of the loop, and could appreciably disturb the flow in the vicinity of the coil. The signal improved as the disturbance of the plasma by the magmetic coil was made smaller. In fact, the best measurements were made with a single turn of wire, either coated or bare, that extended into the plasma, which should produce the smallest disturbance to the flow.

The change in the azimuthal component of magnetic field across the shock, ΔB_θ, was measured with the single turn flux coils. This was done over a wide range of initial pressures at constant Alfven Mach number, $M_A = 2$. The results of these measurements are shown in Fig. 7. The ratio of the measured to the calculated ΔB_θ appropriate for the measured value of M_A is plotted versus the initial pressure, p_1. The initial azimuthal bias field B_{θ_1} was varied from 2500 to 4200 gauss, and the coil diameters ranged from 1 mm to 3.5 mm. The data show that for p_1 below 500μ (which corresponds to shock velocities in excess of 14 cm/μsec) the

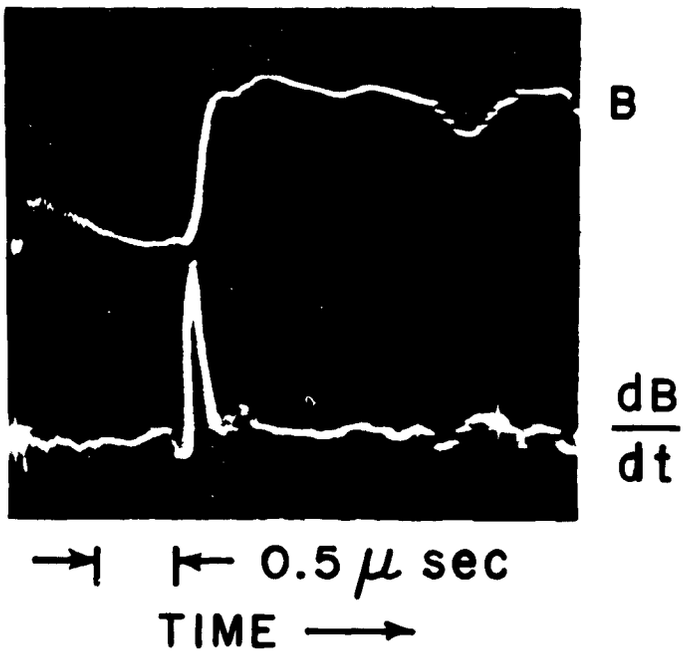

Fig. 6 An oscillogram showing the magnetic field variation with time. An insulated, directly coupled flux coil was used. The top trace is obtained by integrating the signal from the coil, and the bottom trace is the coil signal. The initial pressure for this run was 40μ and the shock velocity was 35 cm/μ sec.

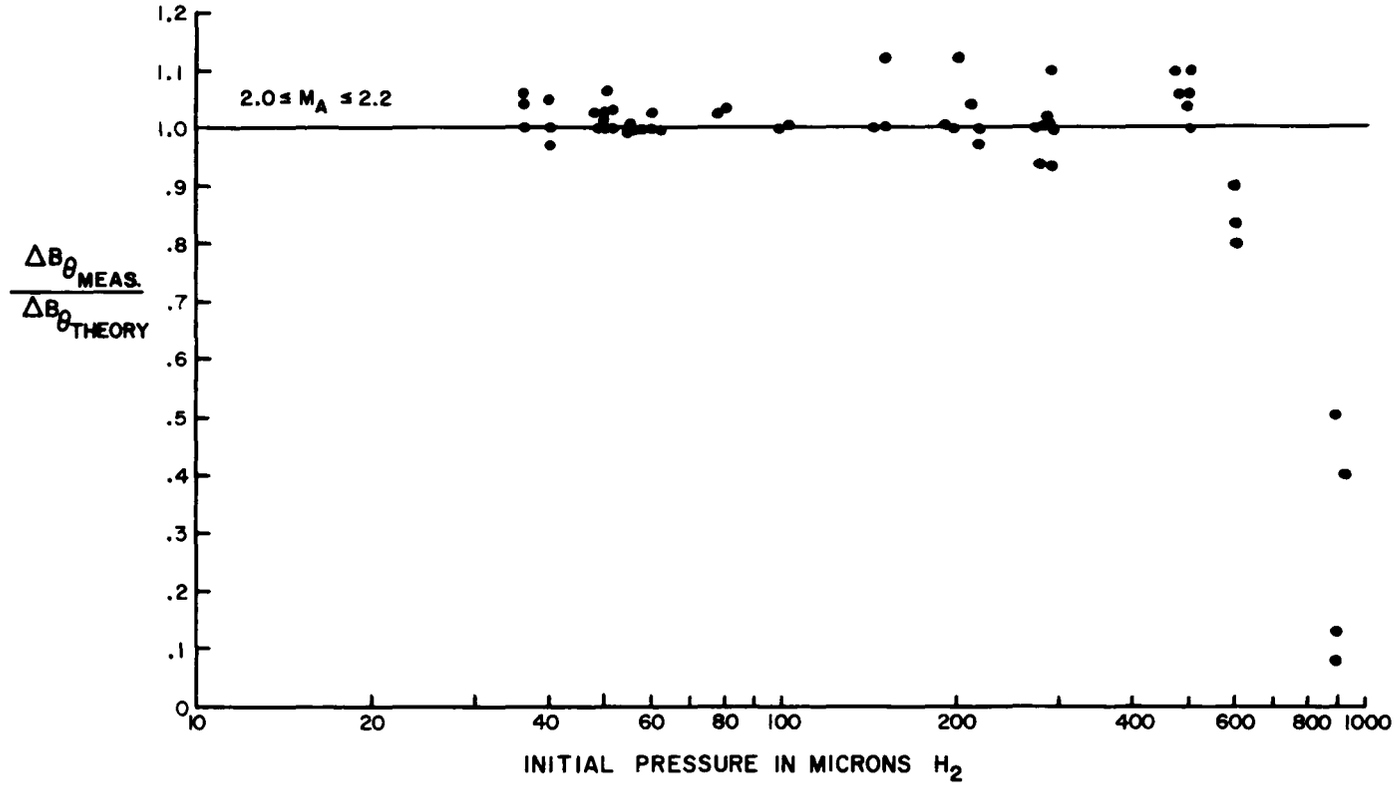

Fig. 7 This is a plot of the ratio between the measured change in B_Θ across the shock to the calculated value. M_A was constant for these shocks within the accuracy of the determination of the shock velocity.

measured change in the field across the shock agrees with the predicted value assuming no leakage of magnetic flux ahead of the shock. For p_1 above 500μ, where the shock velocities were less than 14 cm/μsec, the measured ΔB_θ is less than the computed value. This shows that for these high densities and lower shock speeds the plasma conductivity behind the shock front is insufficient to prevent appreciable diffusion of the magnetic field ahead of the shock.

The final equilibrium enthalpy behind the shock for values of p_1 above 500μ is insufficient to totally ionize the plasma. Furthermore, for p_1 above 800μ the calculated plasma conductivity behind the shock is low enough to allow the magnetic field to diffuse from the interface to the shock during the test time. The data show that for p_1 below 500μ the plasma properties can be predicted by assuming that there is no leakage of the magnetic field ahead of the shock.

Heat Transfer Measurements: A new type of heat transfer gauge[14] has been employed that is suitable for measurements on shock tubes and other pulsed plasma devices. During recent years, the use of the resistance gauge for measurements of heat transfer in chemical shock tubes has received wide application. These gauges have sufficient time response and sensitivity, but have limited use in plasma devices because of electrical shorting and pickup. The resistance element comes in contact with the plasma and must operate in regions of strong electromagnetic fields. The heat transfer gauge that we have developed is highly suitable for studying plasma heat transfer, since it is unaffected by strong electromagnetic fields. The basic idea of the gauge is to use a thin opaque layer of carbon to which plasma heating is applied on one side, while the temperature of the other side is determined by its infrared emission. The carbon layer is thin enough so that the temperature of the surface in contact with the plasma can be determined within a fraction of a microsecond.

Figure 8 shows how this gauge is used in shock tubes for heat transfer measurements. A portion of the shock tube wall is replaced with a heat transfer gauge, which consists of a layer of carbon (1000A to 8000A thickness) deposited on sapphire. Energy from the shock heated gas is transferred to the gauge. Changes in the infrared radiation from the back sur-

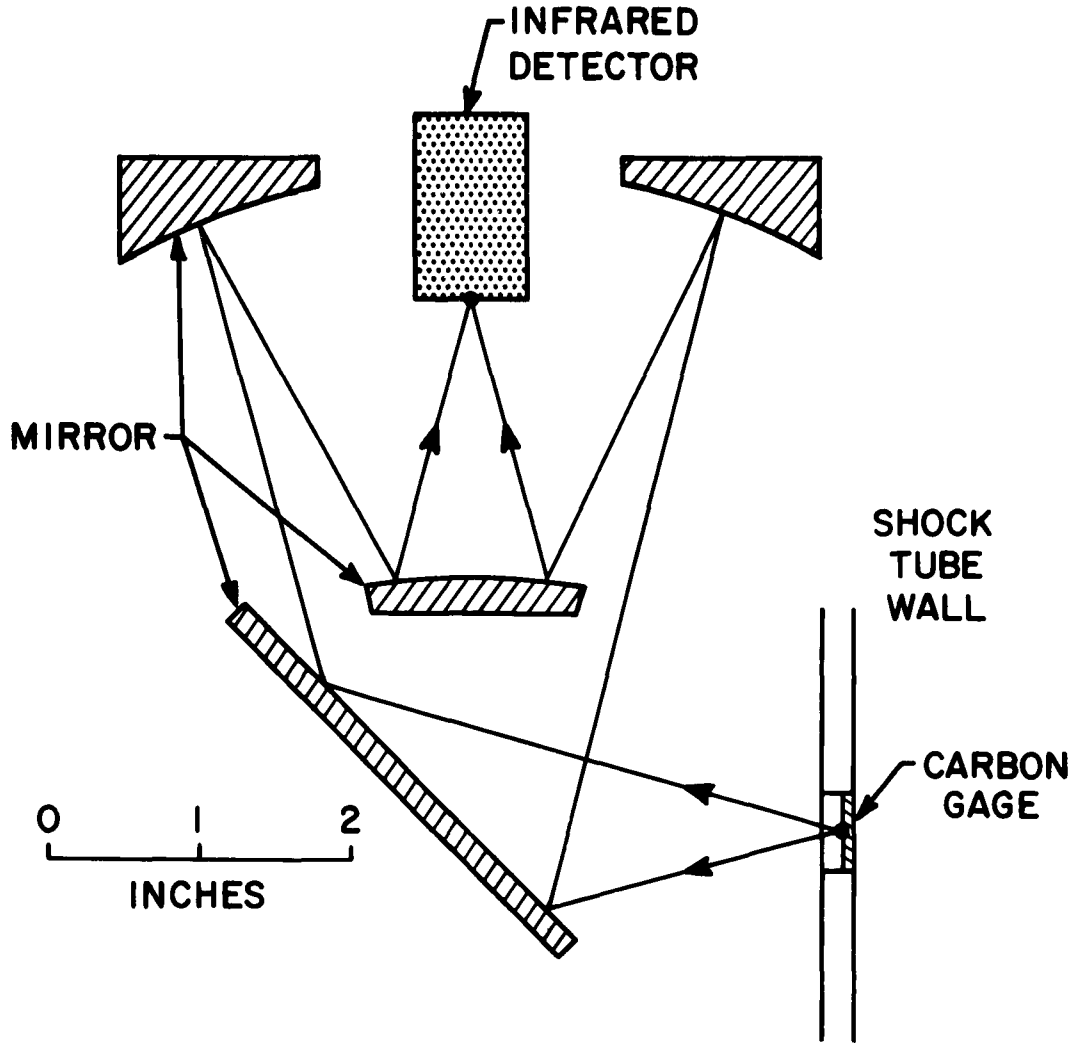

Fig. 8 This is the infrared gauge arrangement for measurements of heat transfer to the shock tube wall.

face of the carbon are observed with a Westinghouse gold-doped germanium detector. An f:2 Cassegrainian optical system using mirrors images the gauge on the I. R. detector.

Two methods have been used to calibrate this infrared heat transfer system. In the first method, the temperature of the gauge is fixed and its infrared emission is measured with the same optical system and electronics as is used for obtaining the experimental data on the MAST. Figure 9 shows a calibration curve of the output signal in millivolts as a function of the gauge temperature.

The second calibrating method, which is more direct, uses shock heated air for a short calibrated heat pulse. The air heat transfer rates have been measured by other methods,[15] and the theory is well developed.[16] Figure 10 shows experimental data using an ordinary chemically driven shock tube. The carbon gauge was placed in the end plate and was heated by the air behind the reflected shock. The detector output is shown as a function of time. Note that the gauge signal rises sharply and levels off. The effect of the interaction between the driver gas and the reflected shock appears after 15 microseconds. The temperature of the end plate should jump to a constant value for aerodynamic heat transfer; thus, the infrared emission should be constant. The time for the infrared emission to reach a constant value is of the order of $\frac{1}{2}$ microsecond or longer depending upon the thickness of the carbon layer. Thinner carbon layers (having less than $\frac{1}{2}$ microsecond rise time) become transparent and the infrared radiation from the gas swamps the emission from the carbon layer. In order to reduce the gauge response time below $\frac{1}{2}$ microsecond, the sapphire was coated with a double layer. A thin layer of carbon was first evaporated on a highly polished sapphire surface on which an opaque thin layer of aluminum was overcoated. The aluminum is made thin enough so that the heat capacity of the carbon layer is not affected.

For the experimental data shown in Fig. 10, the aerodynamic heating rate is $q(t) = Q/\sqrt{t}$, where Q is a constant and t is the time. Figure 11 shows the theoretical time variation of the temperature of the back surface of the carbon in terms of the thermal transit time τ of the carbon layer, where

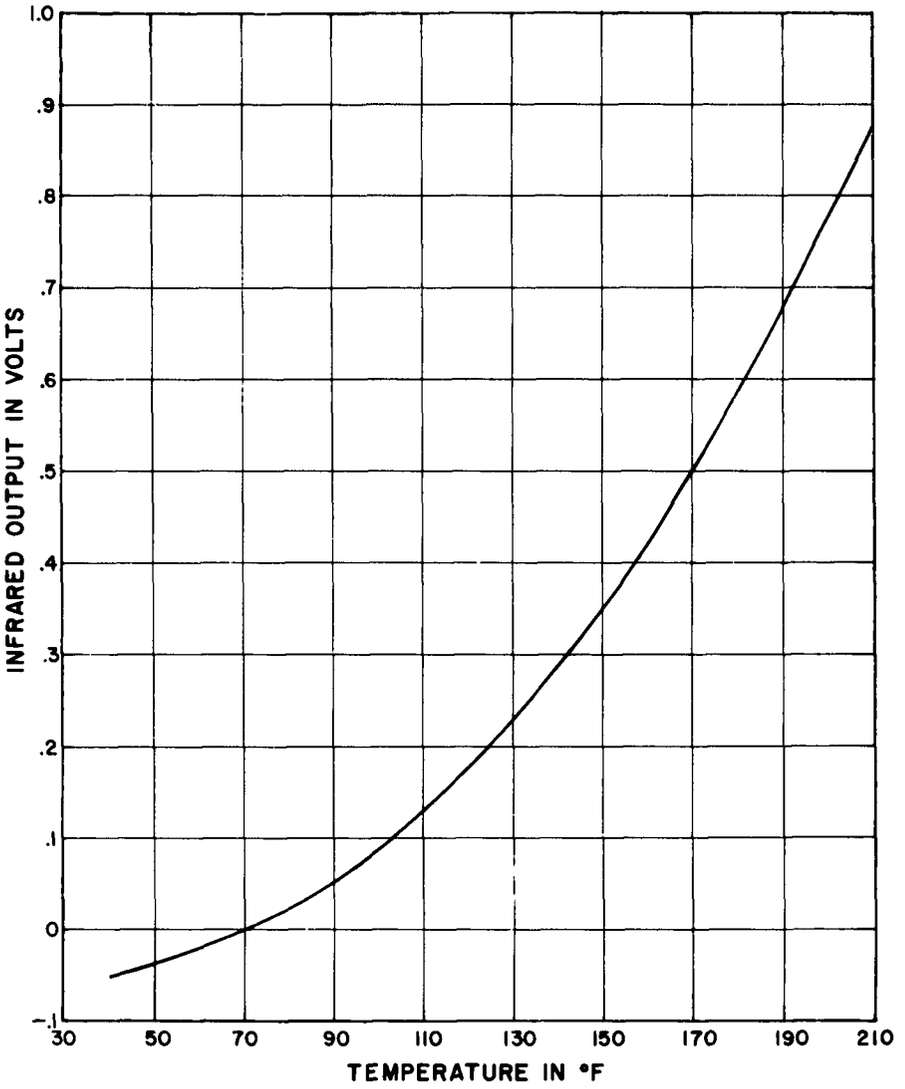

Fig. 9 Calibration curve for the infrared heat transfer gauge. The output of the system in volts is plotted as a function of the gauge temperature in degrees fahrenheit. The gauge is maintained at a constant temperature during the calibration. A small correction was made which took into account the radiation from the sapphire. For very short pulses, the temperature of the opaque carbon layer changes during the heat pulse, but essentially all the sapphire remains at room temperature.

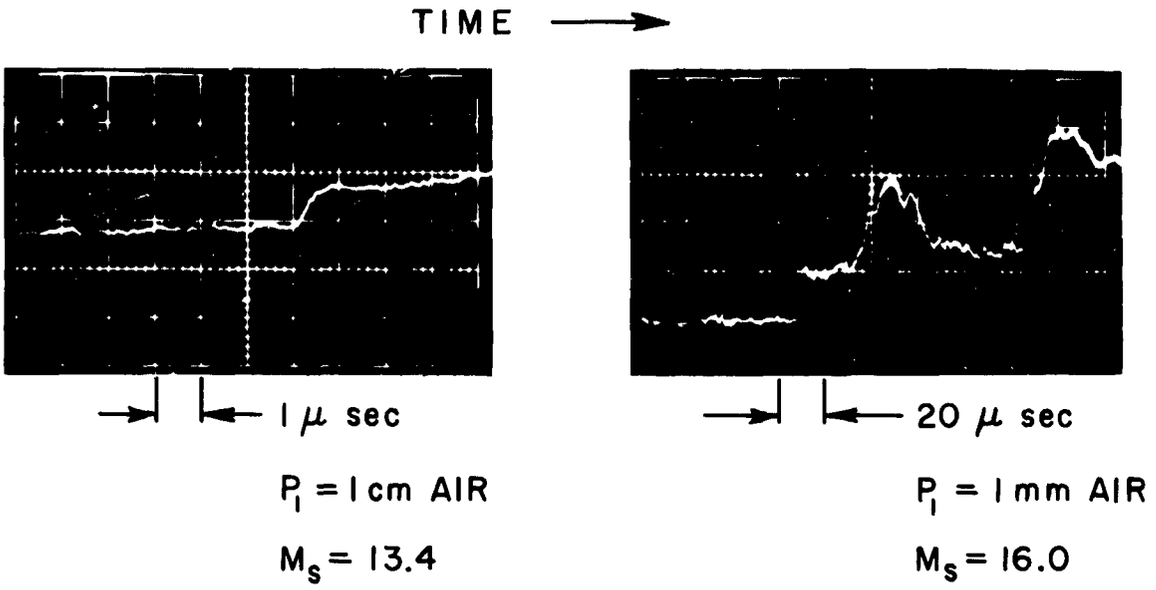

Fig. 10 These are heat transfer measurements on the end plate (reflected shock conditions) of a chemically driven shock tube. The oscillograms show the infrared gauge output versus time. M_s is the incident normal shock Mach number and p_1 is the initial air pressure.

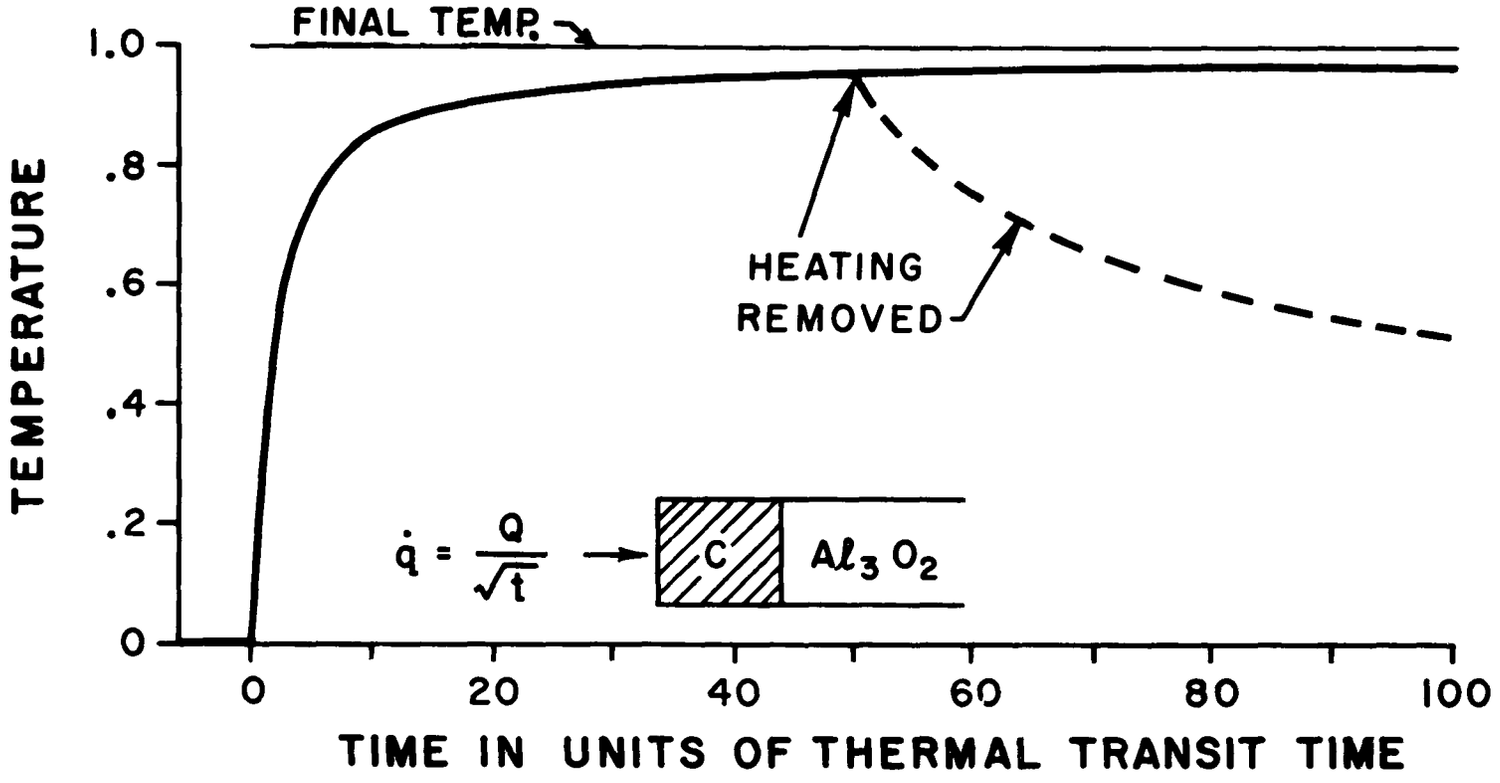

Fig. 11 The variation of the temperature at the back of the carbon layer with time for a laminar heat transfer; $\dot{q}(t) = Q/\sqrt{t}$. The heat transfer gauge consists of a carbon coating on sapphire. The origin is at the time of shock arrival at the gauge. Also shown is the temperature variation at the back of the carbon after the heating is removed.

$\tau = \ell^2/4\kappa$. ℓ and κ are the thickness and thermal diffusivity of the layer. This theoretical curve is correlated to the voltage pulse shown in Fig. 10 with the use of the calibration curve shown in Fig. 9.

Figure 12 shows a comparison of the experimental air data to theory. The lines are the theory and the bars are the experimental points obtained with the present heat transfer gauge. The theory is an extension of the Fay-Riddell[16] stagnation heat transfer by N. H. Kemp.[17] This comparison of the I. R. gauge to the work of others using another method gives us confidence in its application for pulsed experiments.

The heat transfer measurements obtained in the MAST are shown in Fig. 13. The carbon was placed flush with the inside wall of the outer tubing. Data for two consecutive runs are shown. The circuit rise time was approximately 0. 3 microsecond and the aluminum plus carbon coated gauge had 0. 1 microsecond rise time. The peak signal corresponds to a temperature change of 90°F. Note that the heating stops after about $\frac{1}{2}$ microsecond corresponding to the time of passage of the shock heated gas. The expected temperature variation with time is shown by the dash curve in Fig. 11.

The gauge temperature rise is plotted as a function of the shock velocity in Fig. 14. It should be noted that for shock velocities above 20 cm/microsecond, the shock heated gas is in the collision-free regime. Based on these temperature rises, the thermal boundary layer thickness can be computed. This is the equivalent thickness of free stream gas that has the energy equal to that deposited on the wall. This thickness decreases from 2 mm to 1 mm with increasing shock velocity. The free stream gas energy consists of the gas enthalpy and directed kinetic energy (in laboratory coordinates). If the magnetic energy density were included in the free stream energy density, then the thermal boundary layer thickness would be reduced by a factor of 3.

The measured thickness may be an upper limit to the actual boundary layer thickness, since a 6 mm diameter non-conducting gauge was used for the measurements. The magnetic lines can leak into this electrical hole causing additional plasma to flow to the surface. Ablation of material from the shock tube wall might also affect the heat transfer measurements by shielding the plasma from the gauge. These measurements are preliminary

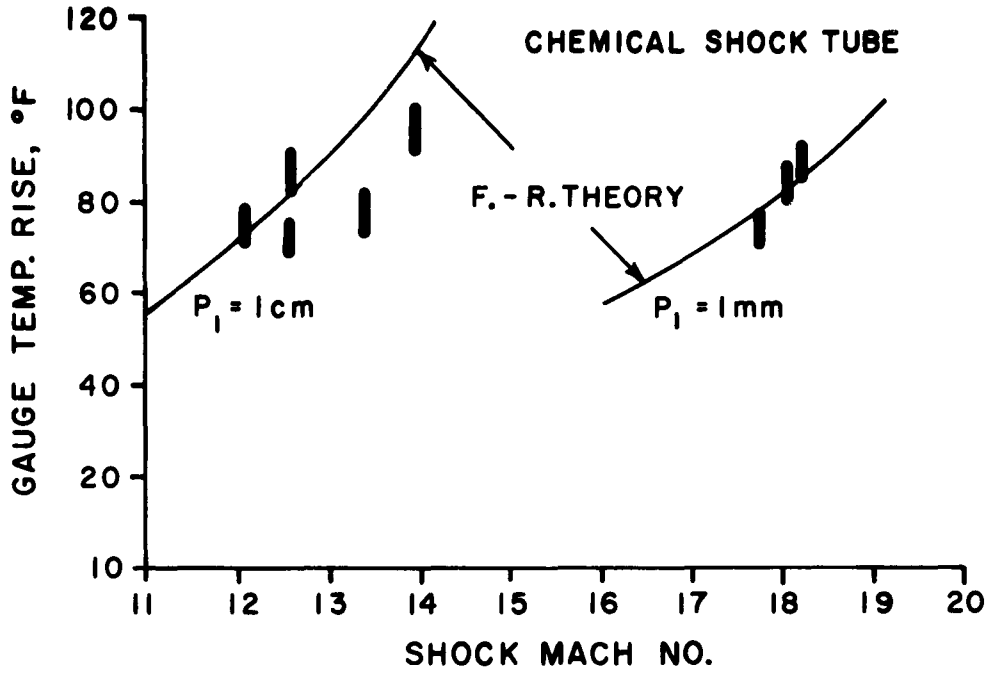

Fig. 12 This is a comparison of experimental measurements of the heat transfer from air to the theory of Fay and Riddell. The measured temperature rise is plotted as a function of the shock Mach number. Measurements were obtained for initial air pressure of 1 cm and 1 mm.

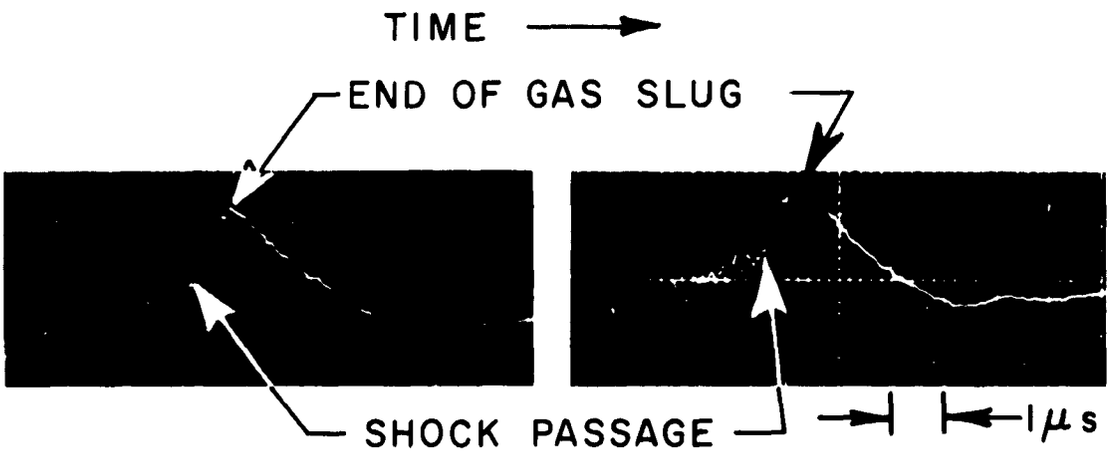

Fig. 13 These are heat transfer measurements on the MAST side wall. Oscillograms showing the infrared gauge output versus time for two consecutive runs. $p_1 = 100\mu$ H_2; $U_s = 13$ cm/μsec; circuit rise time 0.3μsec. The shock arrival time and the end of the heating pulse is indicated.

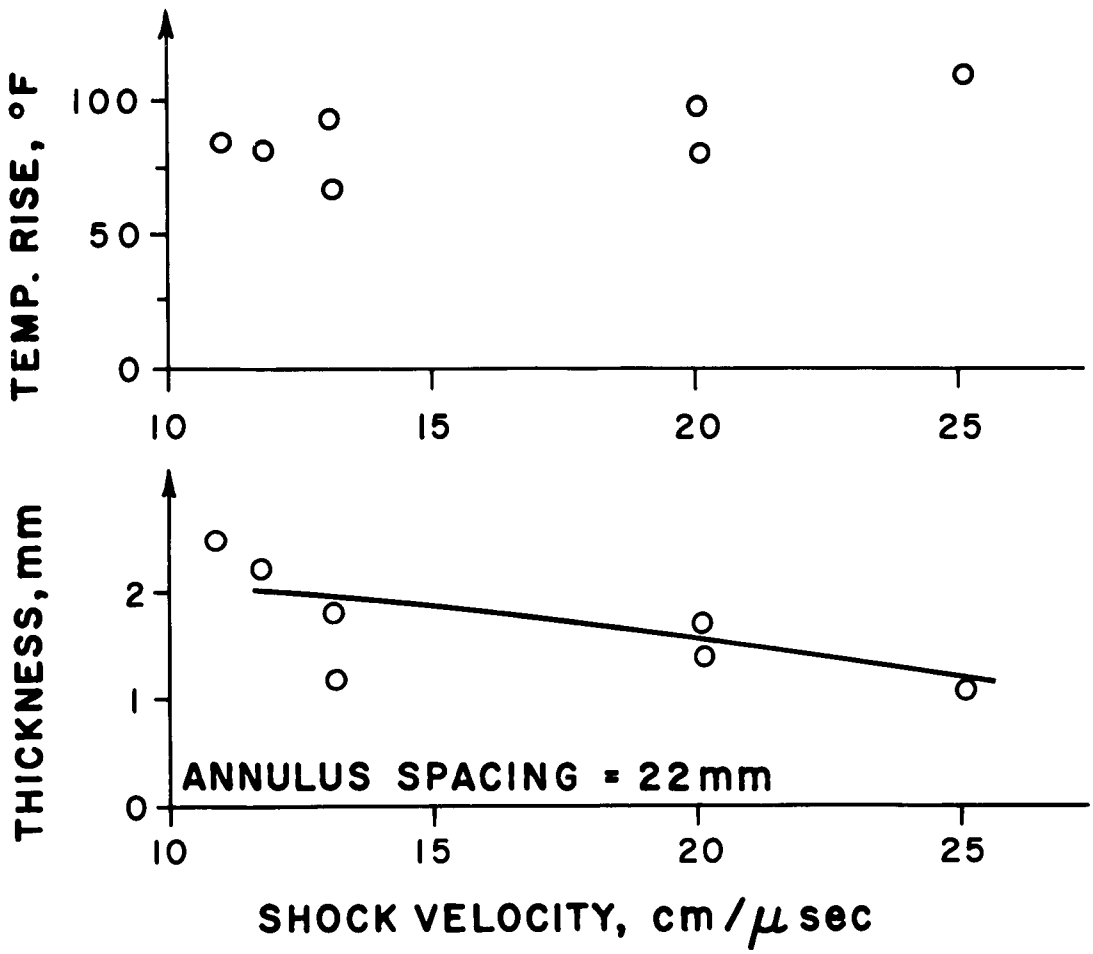

Fig. 14 The top graph presents the experimental results of the gauge temperature rise as a function of the shock velocity. The bottom graph gives the side wall thermal boundary layer thickness after 0.5μsec computed from the gauge temperature rise measurements.

and the effects of holes in the container and wall ablation will be investigated further. It should be noted that the thermal boundary layer thickness is considerably smaller than the annulus spacing of 22 mm that contains the plasma.

Test Time: The test time is the time required for the shock heated plasma to pass over a fixed axial station in the MAST. The length of the plasma that has been shock heated can be obtained from both the radiation measurements, Figs. 3 and 16, and the side wall heat transfer measurements, Fig. 13. This is taken to be the region for which the radiation is constant behind the shock. Test times of 0.4 to 0.6μsec have been obtained with the 15 cm diameter MAST which has a 2.2 cm annulus spacing. Longer test times with the 30 cm diameter MAST have been obtained, which are proportional to the distance the shock has traveled from the electrodes. The test times obtained using the 30 cm MAST have been as long as 2μsec when the quarter cycle time for the drive field is 6μsec. The length of the uniform plasma in both devices is considerably longer than the shock thickness (up to 50 times using the 30 cm MAST). This indicated that the conditions behind the shock can be measured and that these plasma properties can be distinguished from those in the shock wave.

Estimation of Electron Temperature: The electron temperature for initial pressures less than 200μ was estimated with two methods. The first was obtained from the U.V. radiation results, and the second from the measurements of the ratio of hydrogen line intensity to the nearby continuum.

An estimation of the electron temperature was obtained with measurements of the U.V. radiation from about 300A to 1200A with a tungsten photoelectric detector, see Fig. 15. The known photoelectric conversion efficiency for tungsten[10] was used to calibrate the equipment. Some typical oscillograms using this detector are shown in Fig. 16. The circuit rise time for these measurements was less than 0.01 microsecond. The variation of the tungsten gauge output with plasma temperature was obtained by folding the gauge response curve into the plasma radiation intensity. The shock velocity and the Rankine-Hugoniot equations were used to get the electron density behind the shock. This average intensity indicated that the electron

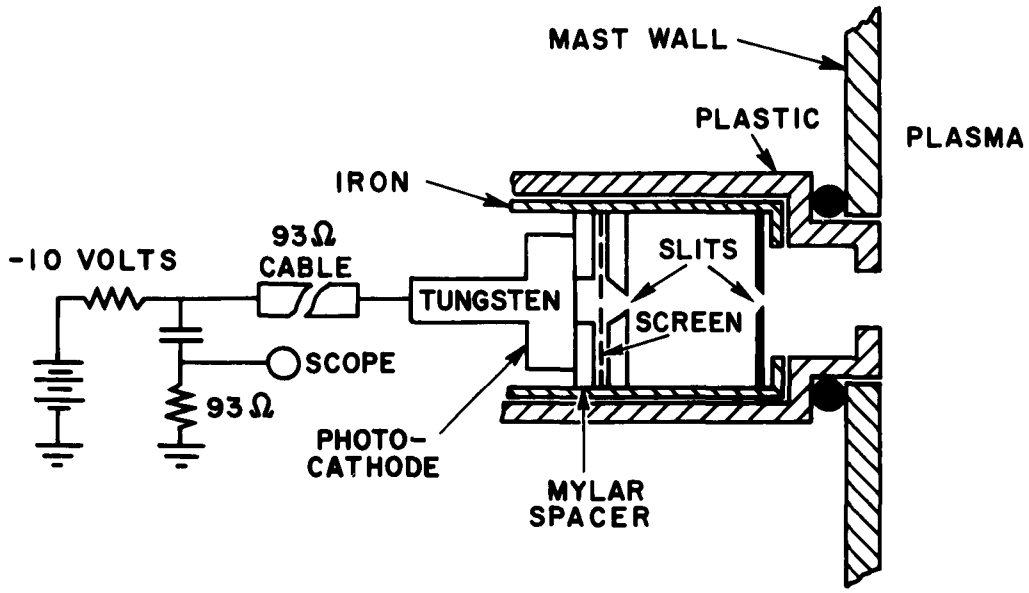

Fig. 15 This is a schematic view of the tungsten U-V detector. The slits determine the optical path; the screen is used to furnish a uniform potential over the tungsten surface.

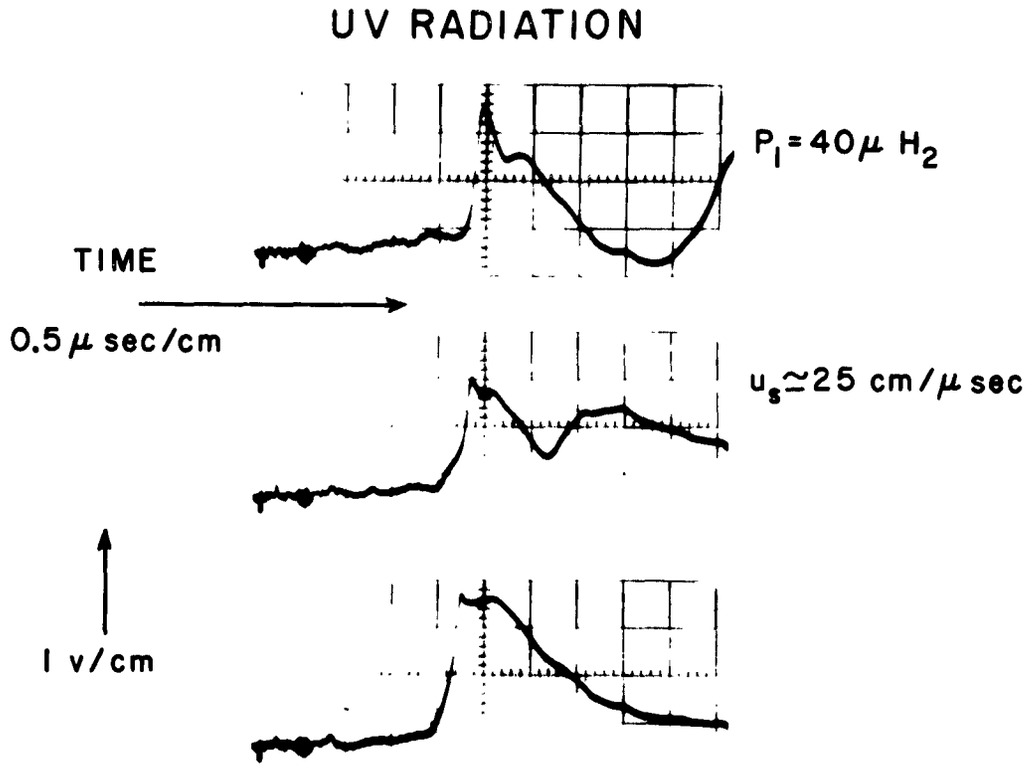

Fig. 16 These are three oscillograms obtained with the tungsten U-V detectors. The voltage is proportional to the radiation for wavelengths between 300A and 1200A.

temperature was greater than 10 volts. This result verifies the use of bremsstrahlung to measure the plasma density in the visible range.

In addition, the temperature of the electrons can be measured by using the ratio of the H_α (6563A) and H_β (4861A) line intensities to the nearby continuum, following a method outlined by Griem.[18] If the hydrogen plasma is sufficiently dense so that the time between collisions of electrons and excited atoms is shorter than the de-excitation time[19] for the excited state, then the line radiation intensity is proportional to the number of atoms in a particular state. The number of atoms in an excited state is proportional to the square of the electron density and so is the continuum intensity. The ratio of the total line intensity and the nearby continuum intensity is therefore, only a function of temperature, except for the correction in the ionization potential. For values of electron temperature, T_e approximately equal to 10 ev, and with electron density, $N_e = 10^{16}/cm^3$, this correction due to the decreased ionization potential is very small and the ratio of the total H_α and H_β line intensities to the nearby continuum is inversely proportional to T_e.

If the shock heated plasma was uniform across the annulus, the method could be used to obtain a close estimate of T_e. The plasma is bounded by two walls and the hydrogen plasma in contact with either wall will be cooler than the interior; hence, the line radiation from these cool boundary layers will be much more intense compared to the continuum than that coming from the plasma in the interior where T_e is high.

Therefore, the results of these measurements obtained with the MAST can be interpreted as lower limits to the value of T_e. These measurements were made with two photomultipliers, a half silvered mirror, and several interference filters. Two of these filters had their maximum transmission on the H_α and H_β lines. The other filters were used to simultaneously measure the continuum between 4400A and 6300A. The bandwidth of the filters ranged between 50A and 100A. These measurements were made with plasma conditions in the MAST such that the initial pressure ranged from 40μ to 100μ of H_2, the shock velocity from 25 to 50 cm/μsec, and the Alfven Mach number from 1.8 to 2.8. Both the ratios of H_α and H_β line intensities to the continuum gave values of T_e approximately equal

to 10 volts. Since small boundary layers with low electron temperatures can effectively reduce the measured T_e with this method, these results cannot be interpreted as a good measure of the shock heated plasma electron temperature, but these results can establish a lower bound of 10 volts to T_e which further confirms the use of bremsstrahlung to measure N_e^2 behind the shock.

Fine Structure Magnetic Field Measurements: Most of the theoretical description[2] of the collision-free shock structure predict the existence of a fine structure to the magnetic field inside the shock. We are attempting to observe the fine structure experimentally. The removal of the quartz envelope around the coil resulted in the successful measurement of the magmetic field jump across the shock. Following this, it was felt that an even smaller disturbance to the plasma would result, if the insulating layer were removed from the exposed single turn coils.

We have used the inductively coupled bare coils to attempt to measure high frequency (in the range from 10 to 100 megacycles) oscillations of the magnetic field in the shock front. The heat transfer to a surface in the shock heated plasma is of the order of 2×10^6 watts/cm^2. The non-conducting material which covers the insulated-directly coupled coil can be ablated during the time required for the shock to propagate past the coil (10^{-1} μsec). This ablated material can form a conducting layer of dense cold plasma around the coil and shield the coil from high frequency changes in the magnetic field. A surface such as copper or tungsten will conduct the heat away from the surface faster than a material such as formvar enamel which was used to cover the insulated coils. An oscillogram which was obtained with a bare coil is shown in Fig. 17. There is a greater indication of high frequency fluctuations of the magnetic field on this picture, compared to the trace obtained with the insulated coil. This bare coil was constructed as shown in Fig. 5 with a glass sting, and with a coil diameter of 1.5 mm. Bare coils with metal stings were also used (Fig. 5), but there was no detectable change in the signal with this type of sting. If the signal from the bare coil on Fig. 17 were to be interpreted as giving actual fluctuations of the magnetic field in the plasma, the fluctuating field would be of the order of 3% of the average field. This 3% fluctuation would be an order of mag-

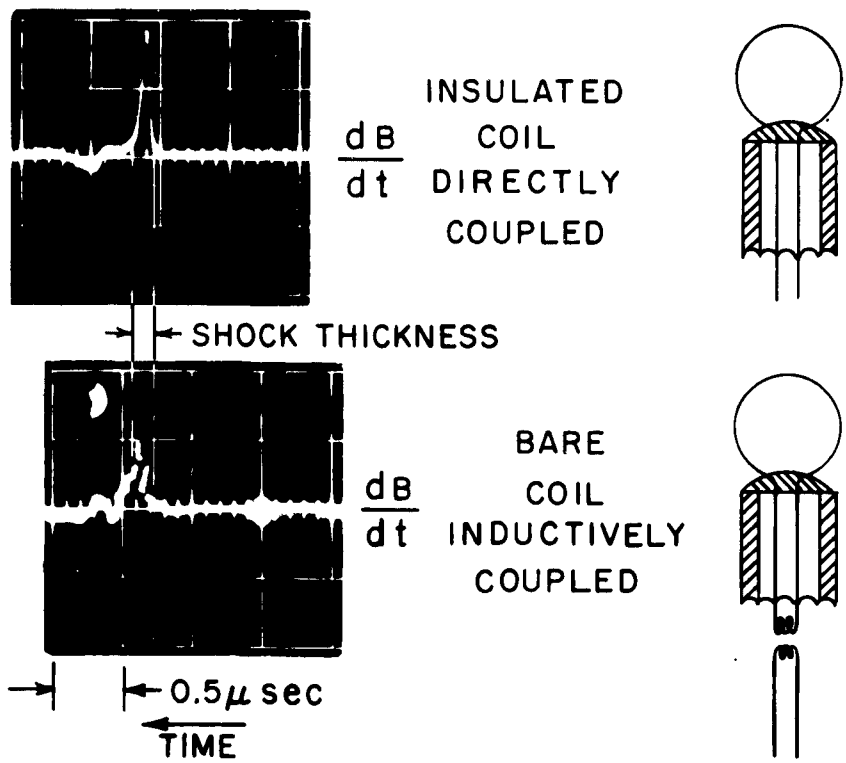

Fig. 17 These two oscillograms were obtained with exposed coils and show the time derivative of the azimuthal magnetic field in the shock. The top trace was obtained with an insulated directly coupled coil, and shows a relatively smooth variation in dB/dt across the shock. The bottom trace was obtained with a small bare inductively coupled coil and shows a noisy variation in dB/dt in the shock.

nitude too small to affect the flow.

Larger diameter (3 to 7 mm), bare coils were also tried, and a typical signal from the large coil is shown in Fig. 18. The integrated signal from this coil (area under the dB/dt trace) gives the correct change in B_θ across the shock. The sudden increase in dB/dt followed by the slow decay indicates that there is some non-linear phenomenon associated with the coil signal. A possible explanation of this signal could be that the coil was shielded from the change in the magnetic field across the shock either by a cloud of ablated material from the coil or by an arc between the two leads of the coil where the coil is connected to the sting. The sudden increase in dB/dt then could correspond to a rupture in the shielding due to the cloud or a break in the arc which allows the compressed field to enter the coil. Furthermore, it must be pointed out that the high frequency oscillations present on the coil signal in Fig. 17 could be due to a series of such effects and not due to a high frequency oscillation in the magnetic field in the shock.

Bare inductively coupled coils did show some indication of a fine structure to the magnetic field in the shock, but at the present time, the interpretation of the high frequency signals from these coils is uncertain.

Summary of Plasma Properties to Show Existence of Shock

It has been previously shown[4] that the shock velocity obtained in a MAST is in agreement with that predicted by using the conservation of mass and momentum equations, the known drive field intensity and the initial conditions ahead of the shock. The measurements of both the plasma radiation, Fig. 4 and the magnetic field, Fig. 7 behind the shock verified the use of the shock mass and momentum equations with infinite electrical conductivity. The measured wall heat transfer, Fig. 14, indicates that during the test time the plasma energy is not lost to the walls. Finally, both the radiation and heat transfer measurements can be used to measure the length of the shock heated plasma region, and this region is long compared to the width of the shock. Therefore, one concludes that very high speed shock waves have been produced, and for low initial pressures ($p_1 \simeq 50\mu$), the energy (thermal and directed) of the shock heated gas is of the order of 10^3 ev per particle.

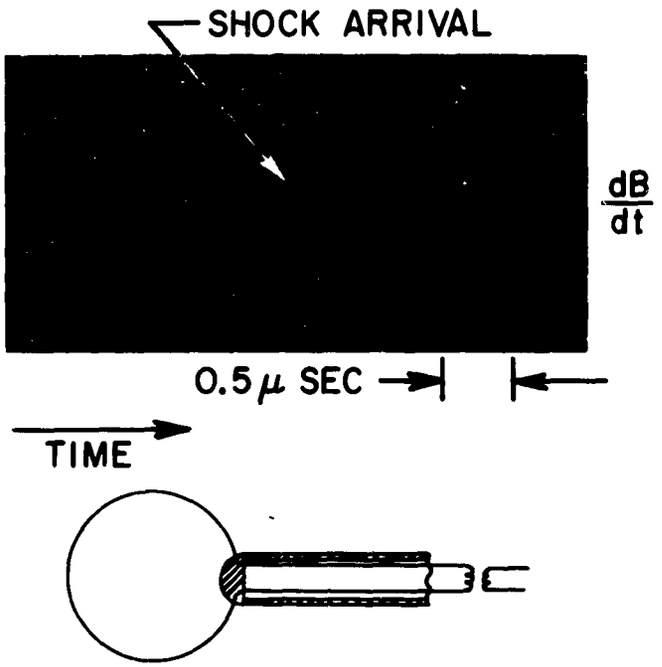

Fig. 18 The oscillogram was obtained with a large (diameter 6 mm) inductively coupled bare coil. The signal shows a rapid rise in dB/dt just after the arrival of the shock followed by smooth decay. This signal is typical of those obtained with large bare coils.

Experimental Collision-Free Shock Thickness

Variation of Shock Thickness with M_A: The Alfven Mach number, M_A, of a magnetically driven shock is a function of the ratio of the total azimuthal magnetic field behind the shock to the field ahead of the shock,[5] i.e., B_0/B_1. A range of values of M_A was obtained by varying B_1 while keeping constant the drive field and the gas density. The shock thickness was obtained from the rise time of the plasma radiation (see Fig. 3). The results of these experiments are shown in Fig. 19 where the measured ratio of the shock thickness to the characteristic ion radius, r_i, is plotted against M_A. r_i is the gyro-radius of a hydrogen ion moving with the Alfven velocity for conditions ahead of the shock. Note that r_i is only a function of the initial density. The data were obtained for initial hydrogen gas pressure p_1 ranging from 70 to 90μ Hg, and for shock velocities in excess of 30 cm/μsec. The ion mean free path, λ, behind the shock was computed as follows: $\lambda = 1/N_i Q_i$, where $N_i = N_e$ = the measured electron number density behind the shock, and Q_i is the Coulomb cross-section for 90° deflections assuming the particles have the equilibrium plasma temperature behind the shock. The equilibrium temperature is obtained by using the energy equation across the shock[5] and the measured shock speeds. Also shown in Fig. 19 is the theoretical estimation[2] of the collisionless shock thickness versus M_A. This calculation gives results which are valid within the approximation of the theory for $M_A \gtrsim 3$.

The ratio of axial to azimuthal magnetic field ahead of the shock for the experiments was equal to 0.365, corresponding to an angle, α, between the plane of the shock front and the magnetic field ahead of the shock of 20°. Experiments have been carried out where α was varied from 10° to 35°, over the same range of M_A as shown on Fig. 19. The measured shock thickness was observed to be independent of α within the experimental scatter.

Variation of Shock Thickness with Density: The variation of the shock thickness with density is shown in Fig. 20. The Alfven Mach number, M_A, was held constant while the initial pressure, p_1, was varied. Since M_A is a function of B_0/B_1 and the density ratio across the shock is a function

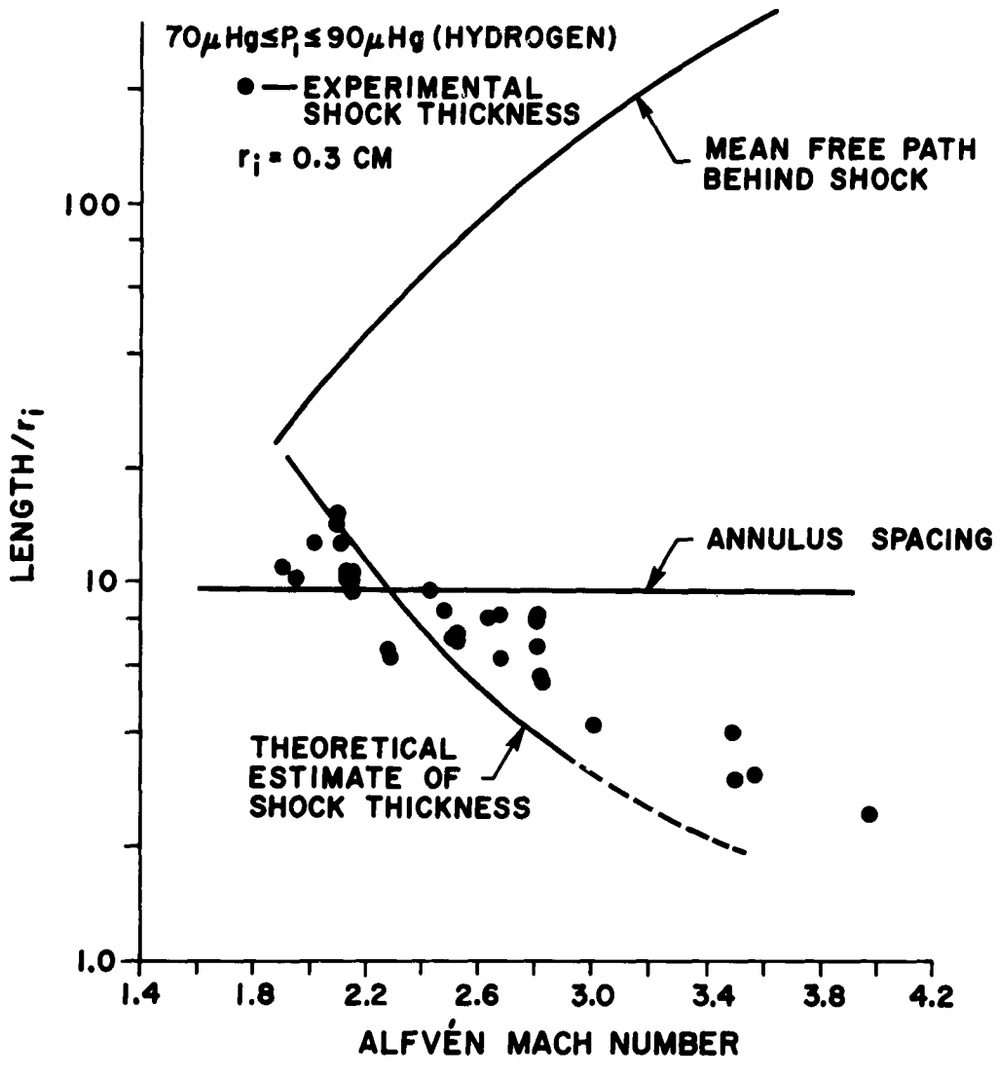

Fig. 19 The experimental shock thickness was obtained by measuring the rise time of the radiation across the shock. This data is shown by the circles. The initial pressure was between 70μ and 90μ, the Alfven Mach number was changed by varying the initial bias field intensity. The characteristic ion Larmor radius, r_1 = 0.3 cm for these experiments.

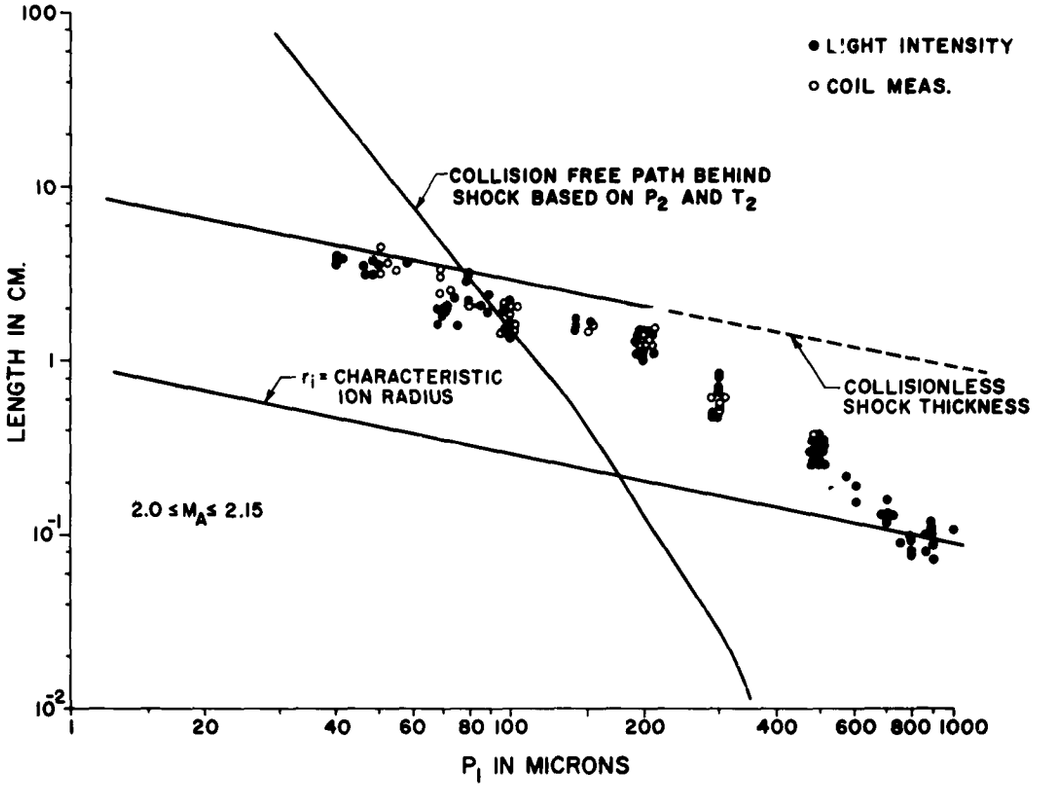

Fig. 20 This is a plot of the measured shock thickness versus the initial pressure in hydrogen. The data was obtained by measuring the rise time of the radiation across the shock (solid circles) and the rise time of the magnetic field compression across the shock measured with the flux coils (hollow circles).

of M_A, a change in p_1 changes the plasma density, temperature behind the shock, shock velocity, and the characteristic ion radius. The solid points on this graph were obtained using the rise time of the radiation emitted by the shock heated plasma, see Fig. 3. The hollow circles denote the results obtained using the single turn flux coils, which measured the rise time of B_θ across the shock, see Fig. 6. The characteristic ion radius is shown along with a theoretical estimate of the shock thickness.[2] The theoretical shock thickness for large mean free paths is equal to 10 r_i for $M_A = 2$. Also shown is the ion collision mean free path, λ, based on the same conditions as shown in Fig. 19. For pressure below 150μ Hg, λ is very nearly proportional to p_1^{-3}. This can be shown as follows: $U_s^2 = k_1 B_0^2/p_1$ and $T_2 = k_2 U_s^2$ where U_s is the shock velocity, T_2 is the equilibrium temperature behind the shock, and k_1 and k_2 are functions of the Alfven Mach number.[5] Since the Coulomb cross-section is proportional to T_2^{-2}, the mean free path varies as p_1^{-3}. For p_1 above 150μ Hg, the energy invested in ionizing the hydrogen is not negligible and T_2 decreases more rapidly with increasing p_1. Hence, for large values of the initial pressure, λ decreases more rapidly with increasing p_1.

The measured shock thickness can be predicted using the theory described in Refs. 1, 2 and 3 up to a value of p_1 where the calculated λ becomes comparable to r_i. At higher values of p_1 the plasma waves which give rise to the collisionless dissipation mechanism are damped due to particle collisions. For values of p_1 greater than 300μ the shock thickness decreases more rapidly with increasing p_1, indicating that collisional processes begin to dominate the shock structure.

CONCLUDING REMARKS

1. A magnetic annular shock tube, MAST, has been developed to the point where it produces shocks with speeds ranging up to 50 cm/μsec. The shock waves produced are identified in the following ways:

   (a) The light intensity behind the shock front agrees with the predicted density behind the shock.

(b) The measured shock velocity agrees with the measured magnetic drive field as is required by conservation of momentum.

(c) The magnetic field compression across the shock wave has been measured and for all cases where the expected gas temperature behind the shock is high enough so that constancy of B_θ/ρ is expected, this constancy is observed. For lower shock velocities where lower temperatures are reached behind the shock, smaller field rises are obtained as expected.

2. A preliminary indication has been obtained that only a small fraction of the plasma energy (about 10%) is lost to the walls. At the higher shock velocities (above 26 cm/μsec) the kinetic energy of the incoming atoms (or ions) is large enough so that the mean free paths for momentum exchange by particle collision are larger than the apparatus dimensions and the ion cyclotron radius. The existence of a shock wave under these conditions is evidence that processes other than a collisional shock are responsible; i.e., that a collision-free shock has been produced experimentally.

3. The thickness of the collision-free shock waves has been measured by the rise time of the light emission in the visible and ultraviolet and by the rise time in magnetic field as measured with search coils. These thicknesses are all in agreement and the dependence of this thickness on initial density and Alfven Mach number has been measured. These measured shock thicknesses are smaller than the channel dimensions for small Alfven Mach numbers and larger than the channel dimensions for larger Alfven Mach numbers. Further, the hot plasma created by these shock waves is observed to persist for times large (up to 50 times) compared to the time of passage through the shock. These measurements are in agreement with a published theory[1, 2, 3] when the characteristic ion cyclotron radius is smaller than the mean free path in the shocked plasma.

REFERENCES

1. Kantrowitz, A.R., Patrick, R.M. and Petschek, H.E., "Collision-Free Magnetohydrodynamic Shock Wave," Paper presented at the 4th International Conference on Ionization Phenomena in Gases, Uppsala, Sweden, August, 1959, pp. 1086-1091.

2. Fishman, F.J., Kantrowitz, A.R. and Petschek, H.E., Rev. Mod. Phys., 32:959 (1960).

3. Camac, M., Kantrowitz, A.R., Litvak, M.M., Patrick, R.M. and Petschek, H.E., "Shock Waves in Collision-Free Plasmas," Paper presented at the International Atomic Energy Agency Conference on Plasma Physics and Controlled Nuclear Fusion Research, Salzburg, Austria, September, 1961.

4. Patrick, R.M., Phys. Fluids, 2:589 (1959).

5. Kemp, N.H. and Petschek, H.E., Phys. Fluids, 2:599 (1959).

6. Marshall, J., "Acceleration of Plasma into Vacuum," Proceedings of the Second United Nations International Conference on the Peaceful Uses of Atomic Energy, Volume 31. United Nations, Geneva. September 1958. pp. 341-347.

7. Alfven, H., Lindberg, L. and Mitlid, P., J. Nucl. Energy, Part C, 1:116 (1960).

8. Patrick, R.M., Bull. APS., 3:39 (January 1958).

9. Keck, J.C., Fishman, F. and Petschek, H.E., Bull. APS., 6:278 (April 1961).

10. Walker, W.C., Wainfan, N. and Weissler, G.L., J. Appl. Phys., 26:1366 (1955).

11. Janes, G.S. and Koritz, H.E., J. Appl. Phys., 31:525 (1960).

12. Karzas, W.J. and Latter, R., "Hydrogenic Bound-Free Gaunt Factors," Rand Corporation Research Memorandum RM-2091-AEC. January 1958.

13. Patrick, R.M., Bull. APS., 6:380 (June 1961).

14. Camac, M. and Feinberg, R., Bull. APS., 6:380 (June 1961). Avco-Everett Research Laboratory, Research Report 120.

15. Rose, P. H. and Stark, W. I., J. Aero. Sci., 25:86 (1958).

16. Fay, J. A. and Riddell, F. R., J. Aero. Sci., 25:73 (1958).

17. Kemp, N. H., Avco-Everett Research Laboratory, Private Communication.

18. Griem, H. R., "Plasma Spectroscopy," Paper presented at the 5th. International Conference on Ionization Phenomena in Gases, Munich, Germany, August-September 1961.

19. Bethe, H. A. and Salpeter, E. E., "Quantum Mechanics of One-and Two-Electron Systems," Handbuch der Physik, Volume 35/1. Springer-Verlag, Berlin. 1957. pp. 88-436.

DISTRIBUTION LIST

AeroChem Research Laboratory - Princeton, New Jersey - ATTN: Dr. H. F. Calcote

Aerojet-General Corp. - San Ramon, California - ATTN: Mr. John Luce

Aeronutronics, Division of the Ford Motor Co. - P.O. Box 697 - Newport Beach, Calif. - ATTN: Library

Allison Division - General Motors Corporation - Indianapolis 6, Indiana - ATTN: Mr. T. L. Rosebrock

Armour Research Foundation - 10 West 35th St. - Chicago 16, Ill. - ATTN: R. L. Watkins

Arnold Engineering Development Center - ATTN: AEGP AEO - Arnold Air Force Station, Tenn.

Atlantic Research Corp. - Alexandria, Va. - ATTN: Dr. R. Friedman

AVCO-Everett Research Laboratory - 2385 Revere Beach Parkway - Everett 49, Mass. - ATTN: Dr. A. R. Kantrowitz

AVCO-Everett Research Laboratory - 2385 Revere Beach Parkway - Everett 49, Mass. - ATTN: Dr. R. Patrick

AVCO-Everett Research Laboratory - 2385 Revere Beach Parkway - Everett 49, Mass. - ATTN: Dr. S. Janes

California Institute of Technology - Pasadena, Calif. - ATTN: Mr. Marble

University of California - Berkeley, California - ATTN: Professor L. Talbot

Air Force Cambridge Research Center - Geophysics Division - Laurence G. Hanscom Field - Bedford, Mass. - ATTN: Morton A. Levine

Chicago Midway Labs - Chicago, Ill. - ATTN: P. J. Dickerman

University of Chicago - Chicago, Ill. - ATTN: Mr. T. Bonin

Columbia University - New York, New York - ATTN: Dr. Robert Gross

Cornell University - Ithica, N. Y. - ATTN: Dr. W. R. Sears

Electro-Optical Systems, Inc. - 125 N. Vinedo Ave. - Pasadena, Calif. - ATTN: Mr. Webb

General Electric Co. - Evendale, Ohio - ATTN: Dr. M. L. Ghai

General Electric - Philadelphia, Pa. - ATTN: G. W. Sutton

Litton Industries - 336 No. Foothill Rd. - Beverly Hills, Calif. - ATTN: Mr. E. L. DeGraeve

University of Maryland - College Park, Md. - ATTN: Dr. J. M. Burgers

Massachusetts Institute of Technology - Cambridge 39, Mass. - ATTN: Library

University of Minnesota - Minneapolis, Minn. - ATTN: Dr. E. R. Eckert

National Bureau of Standards - Washington 25, D. C. - ATTN: Dr. C. M. Tchen

Northwestern University - Evanston, Ill. - ATTN: Mr. A. B. Cambel

Ohio State University - Columbus, Ohio - ATTN: Library

Pennsylvania State University - University Park, Pa. - ATTN: Dr. H. Li

Princeton University - Princeton, N. J. - ATTN: Dr. S. M. Bogdonoff

Radio Corporation of America - Princeton, N. J. - ATTN: Dr. Hutter

Rand Corporation - 1700 Main St. - Santa Monica, Calif.

Reaction Motors Division - Thiokol Chemical Corp. - Denville, N. J. - ATTN: Dr. Wolfhard

Republic Aviation Corp. - Conklin St. - Farmingdale, LI, NY - ATTN: Mr. A. E. Kunen

Rocketdyne - Canoga Park, California - ATTN: Dr. R. Boden

University of Southern California - Los Angeles 7, Calif. - ATTN: Dr. R. L. Chuan

Space Technology Laboratories - P. O. Box 95001 - Los Angeles 45, Calif. - ATTN: Dr. David B. Langmuir

Stevens Institute of Technology - Hoboken, N. J. - ATTN: Dr. W. Bostick

Temple University - Philadelphia, Pa. - ATTN: Dr. Lloyd Bohn

Texaco Experiment, Inc. - Richmond 2, Va. - ATTN: Dr. King

Thompson Products, Inc. - 23555 Euclid Ave. - Cleveland 17, Ohio - ATTN: Mr. S. H. Fairweather

Prof. Osman Mawardi - Case Institute of Technology - Cleveland, Ohio

The Warner & Swasey Co. - Control Instrument Div. - 34 West 33rd St. - New York, New York - ATTN: Mr. R. H. Tourin

Aeronutronics, Division of the Ford Motor Co. - P. O. Box 697 - Newport Beach, Calif. - ATTN: Dr. R Hoglund

Aerojet General Corp. - Azusa, California - ATTN: Dr. Himricks

University of Maryland - College Park, Maryland - ATTN: Mr. H. R. Griem

Plasmadyne Corp. - Santa Ana, Calif. - ATTN: Mr. A. C. Ducati

Plasmadyne Corp. - Santa Ana, Calif. - ATTN: Dr. H. G. Loos

United Aircraft Corp. - East Hartford, Conn. - ATTN: Dr. R. G. Meyerand, Jr.

ASD (ASRMPE) Wright-Patterson AFB - Ohio

Applied Mechanics Reviews - Southwest Research Institute - 8500 Culebra Road - San Antonio 6, Texas - (2 copies)

EOAR - The Shell Building - 47 Rue Cantersteen - Brussels, Belgium - (1 copy)

AFOSR (SRLTL) - Holloman AFB - N. Mexico - (1 copy)

AFFTC (Library) - Edwards AFB - California - (1 copy)

AEDC (Library - Arnold AF Stn - Tennessee - (1 copy)

U. S. Naval Research Laboratory Library - Washington 25, D. C. - (1 copy)

ARL (TECHNICAL LIBRARY) - Building 450 - Wright-Patterson AFB - Ohio - (1 copy)

AFSWC (Library) - Kirtland AFB - N. Mexico - (1 copy)

Signal Corps Engineering Laboratory - (SIGFM/EL-RPO) - Fort Monmouth, New Jersey - (1 copy)

Jet Propulsion Lab (NASA) - CIT - Pasadena, California - (1 copy)

Director, Ballistics Research Lab - Aberdeen Proving Ground - Aberdeen, Maryland - (1 copy)

Army Research Office - Duke Station - ATTN: CRD-AA-IP - Durham, N. C. - (1 copy)

Naval Ordinance Laboratory - ATTN: Library - White Oak, Silver Spring, Maryland - (1 copy)

National Bureau of Standards - ATTN: Library - Washington 25, D. C. - (1 copy)

AFSC (BSD) - ATTN: Library - AF Unit PO - Los Angeles 45, California - (1 copy)

Chief of Naval Research - Dept. of Navy - ATTN: Library - Washington 25, D. C. - (1 copy)

AFOSR (SRHP) - OAR - Washington 25, D. C. - (1 copy)

Naval Bureau of Weapons - ATTN: Library - Washington 25, D. C. - (1 copy)

U. S. Atomic Energy Commission - Tech Information Service - 1901 Constitution Avenue - Washington 25, D. C. - (1 copy)

Commanding Officer - White Sands Proving Ground - ATTN: Library - White Sands, N. Mexico - (1 copy)

ASD (RRLN) - Wright-Patterson AFB - Ohio

ASD (ASRC) - Wright-Patterson AFB - Ohio

ASD (ASRNE) - Wright-Patterson AFB - Ohio

ASD (ASRMD) - Wright-Patterson AFB - Ohio

ASTIA (TIPCR) - Arlington Hall Station - Arlington 12, Virginia - (10 copies)

OTS, Dept. of Commerce - Technical Reports Branch - Washington 25, D. C. - (1 copy)

AFOSR (SRGL) - Washington 25, D. C. - (2 copies)

RAND Corporation - 1700 Main Street - Santa Monica, California - (2 copies)

National Aeronautics & Space Administration - ATTN: Library - 1520 H Street, N. W. - Washington 25, D. C. - (1 copy)

Ames Research Center (NASA) - ATTN: Technical Library - Moffett Field, California - (1 copy)

High Speed Flight Station (NASA) - ATTN: Technical Library - Edwards AFB - California - (1 copy)

Langley Research Center (NASA) - ATTN: Technical Library - Langley AFB - Virginia - (1 copy)

Chairman - Canadian Joint Staff (DRB/DSIS) - 2450 Massachusetts Avenue, N. W. - Washington, D. C. - (1 copy)

Marshall Space Flight Center - ATTN: Library - Huntsville, Alabama - (1 copy)

AFSC (SCRS) - Andrews AFB - Washington 25, D. C.

AFCRL (Library) - L. G. Hanscom Field, Massachusetts - (1 copy)

Lewis Research Center (NASA) - ATTN: Technical Library - 21000 Brookpark Road - Cleveland 35, Ohio - (1 copy)

Wallops Station (NASA) - ATTN: Technical Library - Wallops Island, Virginia - (1 copy)

Institute of Technology (AU)Library - MCLI-LIB - Bldg. 125 - Area B - Wright-Patterson AFB - Ohio (1 copy)

ASD (Lib) - Wright-Patterson AFB - Ohio - (1 copy)

ARGMA(ORDXR-OTL) - Redstone Arsenal - Alabama - (1 copy)

Chief, R&D - Dept. of the Army - ATTN: Scientific Information Branch - Washington 25, D. C. (1 copy)

Institute of the Aeronautical Sciences - 2 East 64th Street - New York 21, New York (1 copy)

Avco-Everett Research Laboratory, Everett, Massachusetts. EXPERIMENTAL INVESTIGATION OF COLLISION-FREE SHOCKS AND PLASMAS, by R. M. Patrick and M. Camac. September 1961. 38 p. incl. illus. (Project No. 9751; Task No. 37510) (Avco-Everett Research Report 122; AFOSR 2266) (Contract AF 49(638)-61)

Unclassified report

Investigation of the structure of a shock wave provides an excellent opportunity for studying the dissipation process in collision-free plasmas. The thickness of collision-free shock waves was previously obtained from measurements of the light emitted by the plasma in a magnetic annular shock tube. The magnitude of the shock thickness, and its Mach number and density dependence were in agreement with a theoretical estimate based on the concept that the required dissipation in the shock is produced by non-linear interactions between magnetohydrodynamic waves. Further confirmation of these results has been obtained. A. Measurements of the magnetic field have shown that the magnitude of the field change across

(over)

UNCLASSIFIED

1. Plasma, Collision-Free-Shock-Waves.
2. Shock Waves-Thickness.
3. Plasma Ionized-Shock Waves.
I. Title.
II. Patrick, R. M.
III. Camac, M.
IV. Avco-Everett Research Report 122.
V. AFOSR 2266.
VI. Contract AF 49(638)-61.

UNCLASSIFIED

Avco-Everett Research Laboratory, Everett, Massachusetts. EXPERIMENTAL INVESTIGATION OF COLLISION-FREE SHOCKS AND PLASMAS, by R. M. Patrick and M. Camac. September 1961. 38 p. incl. illus. (Project No. 9751; Task No. 37510) (Avco-Everett Research Report 122; AFOSR 2266) (Contract AF 49(638)-61)

Unclassified report

Investigation of the structure of a shock wave provides an excellent opportunity for studying the dissipation process in collision-free plasmas. The thickness of collision-free shock waves was previously obtained from measurements of the light emitted by the plasma in a magnetic annular shock tube. The magnitude of the shock thickness, and its Mach number and density dependence were in agreement with a theoretical estimate based on the concept that the required dissipation in the shock is produced by non-linear interactions between magnetohydrodynamic waves. Further confirmation of these results has been obtained. A. Measurements of the magnetic field have shown that the magnitude of the field change across

(over)

UNCLASSIFIED

1. Plasma, Collision-Free-Shock-Waves.
2. Shock Waves-Thickness.
3. Plasma Ionized-Shock Waves.
I. Title.
II. Patrick, R. M.
III. Camac, M.
IV. Avco-Everett Research Report 122.
V. AFOSR 2266.
VI. Contract AF 49(638)-61.

UNCLASSIFIED

UNCLASSIFIED

the shock agrees with that expected from the conservation equations. Also the distance over which the field changes agrees with the previous shock thickness measurements. B. The electron temperature was estimated to be above 10 electron volts based on the ultraviolet radiation intensity and the ratio of bound-bound and free-free radiation. C. Measurements of the heat transfer from the plasma to the shock tube wall indicates that less than 1/10 of the gas energy is dissipated to the walls; thus, there is good containment of the shock heated plasma for a time large (50 times) compared to the shock rise transit time. The results of these experiments show that the collision-free thickness is inversely proportional to the Alfven Mach number of the shock. The radiation emitted by the shock heated plasma has been measured over a large range in plasma density; these results, together with those for the magnetic field jump across the shock, show that the performance of the MAST can be predicted by a theory which assumes infinite plasma conductivity.

UNCLASSIFIED

UNCLASSIFIED

the shock agrees with that expected from the conservation equations. Also the distance over which the field changes agrees with the previous shock thickness measurements. B. The electron temperature was estimated to be above 10 electron volts based on the ultraviolet radiation intensity and the ratio of bound-bound and free-free radiation. C. Measurements of the heat transfer from the plasma to the shock tube wall indicates that less than 1/10 of the gas energy is dissipated to the walls; thus, there is good containment of the shock heated plasma for a time large (50 times) compared to the shock rise transit time. The results of these experiments show that the collision-free thickness is inversely proportional to the Alfven Mach number of the shock. The radiation emitted by the shock heated plasma has been measured over a large range in plasma density; these results, together with those for the magnetic field jump across the shock, show that the performance of the MAST can be predicted by a theory which assumes infinite plasma conductivity.

UNCLASSIFIED